Metal-Organic Framework Constructed by Copper(I) Cyanide and Ethyl Isonicotinate Through Hydrogen Bonding

Safaa El-din H. Etaiw · Mohamed M. El-bendary

Abstract The reaction of $K_3[Cu(CN)_4]$ and ethyl isonicotinate (EIN) in the presence of Me_3SnCl in H_2O/acetonitrile medium at room temperature affords the 3D-supramolecular coordination polymer (SCP), $\infty\,^3[CuCN\cdot(EIN)]$, **1**. The structure of **1** consists of 1D-zig-zag chains, which extend via the EIN ligands through hydrogen bonds organized in AB 2D-layers. The infinite AB···AB layers are further extended to form a 3D-network via hydrogen bonds and π–π stacking interactions, thus creating wide channels. The emission spectrum of **1** in the solid state reveals a set of high energy and low energy distinct peaks in the visible region at 400–580 nm upon excitation at 280 nm. The luminescence excitation in **1** could be caused by different possible transitions including metal-to-ligand charge transfer (MLCT) or single-metal-centered (MC) transitions.

Keywords Copper cyanide ·
Supramolecular coordination polymer ·
Ethyl isonicotinate · Hydrogen bonding

1 Introduction

The construction of metal–organic frameworks (MOF) via self assembly of appropriate metal ions with predesigned ligands is a subject of currently active research work because of their intriguing topological and special functional properties such as luminescence, redox activity, catalysis and gas storage [1–10]. Many MOF are microporous materials, which are functionally related to zeolites.

The incorporation of CuCN in an MOF is of great interest in view of their appealing structural and photo-luminescent properties, which should lead to interesting new functional materials [11–13]. Pyridine derivatives can be considered, in most cases, as polydentate ligands, which allow a systematic probing of the effect of modifications to the ligand backbone through which the micro architectures of the arrays could be controlled [12–21]. In addition, MOF-containing ligand-based hydrogen bonds (with donor–acceptor capabilities) in the structure allow the connection of MOF via H-bonds thereby increasing dimensionality. These networks may present advantages in the design of new materials due to the fact that H-bonds are more flexible than coordination bonds [22]. In fact hydrothermal processes have been widely used in the preparation of new MOF-containing pyridine derivatives [14, 18, 20]. Furthermore, R_3Sn^+ cations have a good capability of bridging CuCN fragments to produce a limited number of 3D-frameworks [23]. Within these constraints, we have selected ethyl isonicotinate (EIN), which can act as a multidentate ligand with versatile binding and coordination modes, and cyanide as ligands with the Me_3Sn^+ cation to create multi-dimensional hetero bimetallic MOF. Thus, the present study deals with synthesis and characterization of the product of the reaction of $K_3[Cu(CN)_4]$, Me_3SnCl and EIN, which is expected to exhibit strong luminescence for potential use as a luminescent probe.

2 Experimental Section

All chemicals and solvents used in this study were of analytical grade supplied by Aldrich or Merck and used as received except $K_3[Cu(CN)_4]$, which was prepared in the laboratory according to the literature [24]. Microanalyses

S. E. H. Etaiw (✉) · M. M. El-bendary
Chemistry Department, Faculty of Science, Tanta University,
Tanta, Egypt
e-mail: Safaaetaiw@hotmail.com

(C, H, N) were carried out with a Perkin Elmer 2400 automatic elemental analyzer. The IR spectra were recorded on Perkin Elmer 1430 Ratio Recording Infrared Spectrophotometer as KBr discs. Thermogravimetric analysis was carried out on a Shimadzu AT 50 thermal analyzer (under N_2 atmosphere). Electronic absorption spectra as solid matrices and in ethanol in presence and absence of HCl were measured on a Shimadzu (UV-3101 PC) spectrometer. Fluorescence spectra of solids were measured with a Perkin Elmer (LS 50 B) spectrometer.

2.1 Synthesis of [CuCN·EIN] (1)

A solution of 90 mg (0.3 mmol) of $K_3[Cu(CN)_4]$ in 30 mL H_2O was added with gentle stirring to a solution of 189 mg (0.95 mmol) of Me_3SnCl in 10 mL H_2O and 0.15 mL (1 mmol) of ethyl isonicotinate (EIN) in 30 mL acetonitrile. After 1 week yellow needle crystals started to grow from the initially clear solution. After filtration, washing with small quantity of cold H_2O and acetonitrile and drying over night, 46 mg (60.8% based on $K_3[Cu(CN)_4]$) of yellow crystals were obtained. All attempts to synthesize **1** at room temperature in absence of Me_3SnCl have thus far been unsuccessful.

Anal. Calc. for **1** ($C_9H_9O_2N_2Cu$), %: C, 44.9; H, 3.7; N, 11.6. Found: C, 44.4; H, 3.91; N, 11.8.

2.2 Single Crystal Structure Determination

Structural measurement for **1** was performed on a Kappa CCd Enraf–Nonius FR 90 four-circle goniometer with graphite monochromatic MoKα radiation $\{[\lambda MoK\alpha] = 0.71073 \text{ Å}\}$ at 25 ± 2 °C. The structure was solved using direct methods and all of the non-hydrogen atoms were located from the initial solution or from subsequent electron density difference maps during the initial stages of the refinement. After locating all the non-hydrogen atoms in each structure, the models were refined against F^2 first

using isotropic and finally using anisotropic thermal displacement parameters. The positions of the hydrogen atoms were then calculated and refined isotropically, and the final cycle of refinements was performed.

3 Results and Discussion

The room temperature reaction of $K_3[Cu(CN)_4]$, Me_3SnCl and EIN affords yellow crystals of tin free [CuCN·EIN] **(1)**. There are two abnormal features in this reaction; (a) it is formed at room temperature to produce significant amounts of single-phase product and (b) the resulting product is a tin free assembly, **1**, in spite of the presence of Me_3SnCl. It was expected that this reaction should produce a zeolitic-type SCP containing the Me_3Sn cation. Interestingly, replacing EIN by 4-cyanopyridine (cpy), using the same compounds, gave the distorted diamondoid structure $^{\infty}_3$[CuCN·Me$_3$SnCN·cpy] **(1′)**, which exhibits four equivalent and independent, interlocking frameworks [23]. Single crystals of **1′** were obtained by a very slow transfer of Me_3SnCl from the gas phase into a beaker containing an aqueous solution of $K_3[Cu(CN)_4]$ and cpy that was dissolved in a small quantity of MeCN. From the filtrate of this reaction, orange crystals **(2)** resulted after several days. The structure of **2** was identified by X-ray crystallography [23], which indicates that **2** is isostructural to the earlier reported 3D-assembly, [CuCN·cpy] ($^{\infty}_3$[Cu(μ-CN)(μ-cpy)], **2** [25]. Also, an identical product of **1′** was obtained as a polycrystalline precipitate [23] using the same route used to obtain **1**. All attempts to obtain the organotin assembly containing EIN were unsuccessful.

3.1 Crystal structure of [CuCN·($C_9H_9NO_2$)] = [CuCN·EIN], **1**
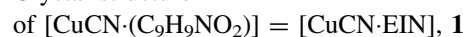
The asymmetric unit of **1** contains one copper atom, one cyanide group and one EIN ligand (Fig. 1). Crystallographic

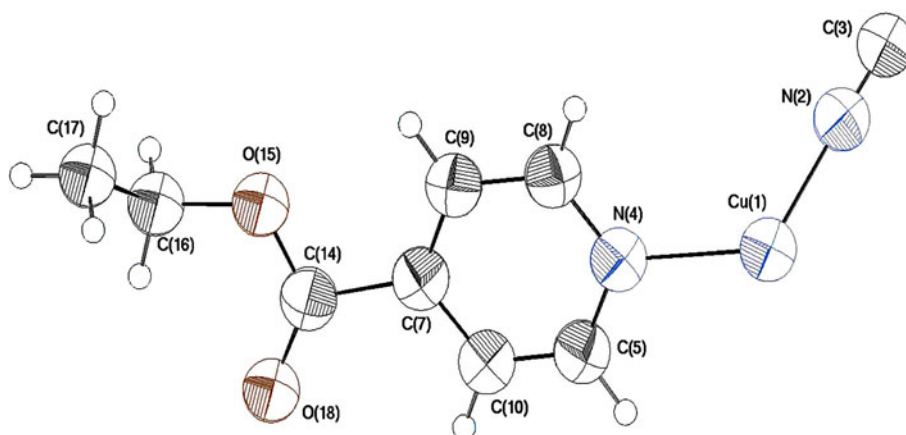**Fig. 1** An ORTEP plot of the asymmetric unit of **1** with atom labeling scheme
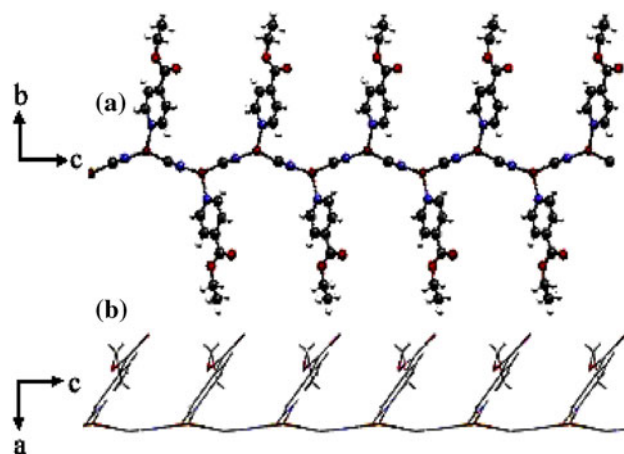
Table 1 Crystal data for **1**

Empirical formula	$C_9H_9O_2N_2Cu$
Formula weight (g/mol)	240.729
Temperature (K)	298
Crystal system	Monoclinic
Space group	C2/c
$a/\text{Å}$	9.6077 (4)
$b/\text{Å}$	23.2584 (11)
$c/\text{Å}$	9.2718 (3)
$\alpha/°$	90.00
$\beta/°$	93.303 (3)
$\gamma/°$	90.00
$V/\text{Å}^3$	2068.43 (15)
Z	8
$\mu(\text{Mo-K}\alpha)/\text{m m}^{-1}$	2.09
Calculated density/g cm^{-3}	1.546
Goodness-of-fit on F^2	5.122
F(000)	1098
R indices[$I > 3\sigma(I)$] R1/wR2	0.095/0.192
R indices(all data)	0.156/0.199
R_{int}	0.026
Data/restraints/parameters	1264/0/86

Table 2 Bond lengths (Å) and bond angles (°) of **1**

Cu1–N4	2.077 (4)	Cu1–Cu1^i	4.0703 (13)
Cu1–N2	1.895 (4)	Cu1–N2^{iv}	3.3254 (7)
Cu1–C3	1.944 (5)	Cu1–N2^{vi}	3.0309 (6)
N2–C3	1.103 (5)		
C14–O15	1.330 (6)	N2–Cu1–N4	121.54 (11)
C14–O18	1.280 (3)	Cu1–N4–C5	119.7 (4)
Cu1–H5	3.015	Cu1–N4–C8	123.7 (3)
Cu1–H8	3.139	Cu1–N2–C3	177.89.7 (3)
Cu1–H17C	2.935	N2–Cu1–C3	138.65 (3)
Cu1–H17B	2.998	C14–O15–C16	113.59 (3)
Cu1–Cu1^{iv}	3.9130 (13)	C7–C14–O18	126.46 (3)

Symmetry codes: (iv) $-x,y,1/2 - z$; (i) $-x,-y,1 - z$; (vi) $x,-y$, $1/2 + z$

Fig. 2 a 1D-zigzag chain with trans EIN ligands in **1** along *a*-axis. **b** 1D-chain with cis EIN ligands in **1** along *b*-axis

Table 3 Hydrogen bond lengths (Å) and bond angles (°) in **1**

D–H···A	d(D–H)	d(H···A)	d(D···A)	∧(DHA)
C8–H8···O18	0.960	2.177	3.034	148.06
C9–H9···O18	0.961	3.071	3.453	105.4
C17–H17A···C17^{ix}	0.960	2.712	3.506	140.44
C10–H10···C10^{ix}	0.960	3.076	3.337	97.25
C16–H16B···N2	0.960	3.191	3.813	124.13

Symmetry codes: (ix) $-x,y,3/2 - z$
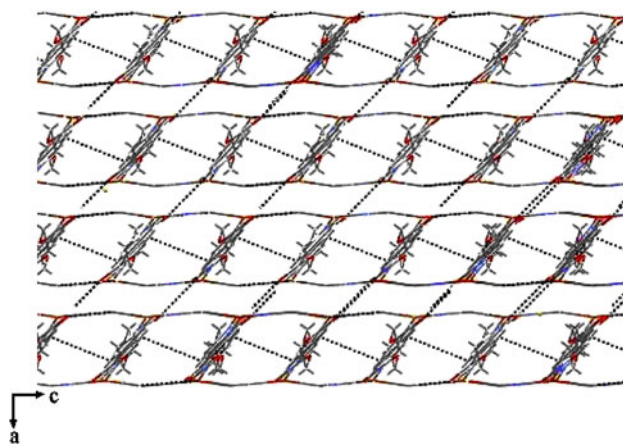
Fig. 3 Infinite AB parallel chains showing hydrogen bonds and channels in **1** along the *b*-axis

data for **1** are summarized in Table 1. Selected bond distances and bond angles are given in Table 2. The copper center forms a trigonal planar geometry via coordination to two cyanide groups and one EIN ligand. The extended structure of **1** along the *a*-axis exhibits a 1D-zigzag chain with *trans* EIN ligands that are present in two planes with an angle of 9.93°. In contrast, the EIN ligands seem to be in *cis* positions along the *b*-axis (Fig. 2). The structure of **1** extends through the EIN ligand to form 2D-layers. Each layer consists of infinite AB parallel CuCN chains along the *b*-axis; the chains are connected by hydrogen bonds between the ethyl

groups with C10-H10 = 3.076 Å and C17-H17A = 2.712 Å (Table 3; Fig. 3). The distance between two copper atoms attached to two facing EIN ligands forming hydrogen bonds is 21.965 Å. The hydrogen bonds connecting the chains form interwoven wide hexagonal $[Cu_6(CN)_4(EIN)_4]$ rings (Fig. 4). Each 2D-layer is further stabilized by extensive hydrogen bonds (2.711–3.076 Å) and π–π stacking
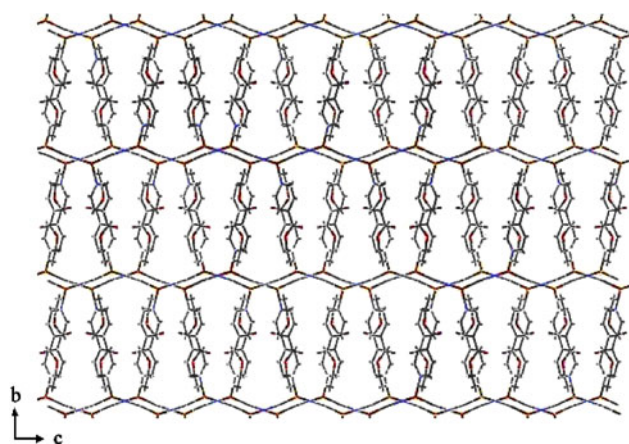
Fig. 4 An interwoven wide hexagonal rings consisting of [Cu$_6$(CN)$_4$(EIN)$_4$] in **1** along the *a*-axis

Table 4 π–π stacking distances (Å) in **1**

C8–O18[iii]	3.034 (4)	C7–O18[x]	3.511 (5)
C14–O18[ix]	3.2947 (5)	C3–C5[i]	3.531 (6)
C10–C10[ix]	3.337 (10)	C7–O18[ix]	3.616 (5)
C9–C9[iv]	3.425 (11)	C5–C10[ix]	3.736 (7)
C8–C8[iv]	3.453 (10)	N4–C8[iv]	3.787 (6)
C9–O18[iii]	3.453 (4)	C5–C5[ix]	3.833 (10)

Symmetry codes: (iii) $1/2 + x, 1/2 − y, z − 1/2$ (ix) $−x, y, 3/2 − z$; (iv) $−x, y, 1/2 − z$; (x) $−1/2 − x, 1/2 − y, 1 − z$; (i) $−x, −y, 1 − z$

(3.337–3.833 Å) (Tables 3, 4). There is no copper–copper interaction in the layers since the nearest distance between Cu1–Cu1 is 3.913 Å. The structure of **1** is further extended to form 3D-infinite AB–AB layers via interlayer hydrogen bonds; (O18···H8 = 2.177 Å, O18···H9 = 3.071 Å, N2···H16 = 3.191 Å) and π–π stacking (3.034–3.833 Å) along the *b*- and *c*-axes (Tables 3, 4). The separation distances between the AB···AB layers are 11.722 Å (C8–C8) and 13.493 Å (Cu1–Cu1) creating wide channels (Figs. 3, 5). Thus, the network structure of **1** may be considered as a good example of a coordination polymer that extends its structure to a 3D open-framework via hydrogen bonds and π–π stacking. The bond lengths around the Cu1 atom are in the normal range reported for prototype compounds [12, 13, 15–17, 19] (Table 5). The N2-Cu1-C3 angle is 136.85°, which causes the zigzag shape of the CuCN chains. Also, the Cu1CN angle (177.89°) deviates slightly from linearity.

Comparing the structure of **1** with **2** ($^3_\infty$[Cu$_2$(CN)(μ-CN)(3-Acpy)$_2$]), **3** ($^3_\infty$[Cu$_2$(CN)(μ-CN)(4-Acpy)$_2$]), **4** (Acpy = acetylpyridine) [13] and **5** ($^3_\infty$[Cu$_2$(CN)(IN)(HIN)]$_n$ (IN = isonicotinate) [19]) indicates that the structures **1**, **3**, **4** and **5** contains three-coordinate Cu(1) while **2** contains tetrahedral Cu(1). The structures of **3** and **4** consist of Cu$_2$CN
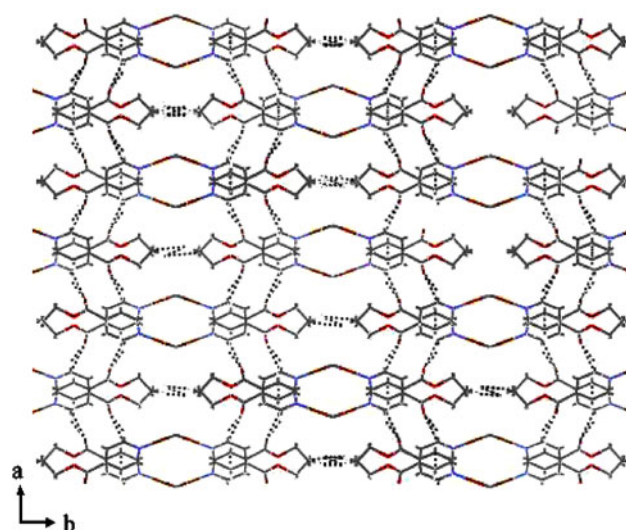

Fig. 5 3D-open framework showing hydrogen bonds in **1** along the *c*-axis

building blocks, which are connected by CN groups to form 1D-zig-zag chains. Each chain in **3** and **4** is bonded to another by hydrogen bonds into a 2D layer. In **3**, however, there is further stacking into an interwoven mode by hydrogen bonds and π–π stacking as well as Cu···Cu interactions to create a 3D-network structure [13]. On the other hand, the structure of **2** consists of 1D CuCN chains connected by the cpy ligand to create a 3D network [25]. The structure of **5**, however, is based on closed [Cu$_6$(CN)$_2$(C$_6$H$_4$NO$_2$)$_2$-(C$_6$H$_4$NO$_2$H)$_2$] distorted fused hexagons while the structure of **1** consists of hydrogen bonded [Cu$_6$(CN)$_4$(EIN)$_4$] fused hexagons. Each closed hexagon unit in **5** is interpenetrated by two others, which extend to a three-fold interpenetrating 2D-network. Each independent 2D-network is hydrogen bonded to only one of the three independent networks of the adjacent layer to give a 3D-supramolecular architecture. In contrast, **1** is constructed of interwoven 2D-layers consisting of hydrogen-bonded hexagons connected by hydrogen bonds to create a 3D-network. Thus, **1** consists of an open non-interpenetrating 3D-framework with wide voids and channels. It is worth mentioning that in the case of pyridine and its methyl derivatives (3-methylpyridine (3-mpy) and 2,4,6-trimethylpyridine (tmpy)) 2D-polymers are formed with the general formula $^2_\infty$[CuCN.0.5 (L)] [12]. Hence, the high dimensional topologies of **1**, **3**–**5** result mainly from extensive hydrogen bonding due to the presence of the acetyl or the carboethoxy group while the presence of the cyanide group in cpy favors the formation of tetrahedral geometry around the Cu(1) site via the bridging capability of the cpy ligand. Such non-interpenetrating networks that contain MOF connected by unconventional H-bonds to build flexible networks should provide a concrete route to porous materials.

Table 5 Bond lengths (Å) of Cu–N(L) and bond angles of L–Cu–(CN)/L–Cu–(NC) (°) of different CuCN compounds

Compounds	Cu–N(base)	L–Cu–(CN)	L–Cu–(NC)	Ref.
[Cu CN·2(py)]	2.10(1)	107.3(6)	110.3(6)	[16]
[(Cu CN)$_2$·3(2-mp)]	2.16(4)	128. (2)	104(2)	[16]
[(Cu CN)$_2$·3(4-mp)]	2.161(7)	104.3(8)	108.7(3)	[17]
[Cu CN·quin]	2.07(1)	120.2(4)	107.3(4)	[16]
[Cu CN·(NHEt$_2$)]	2..09(1)–2.11(1)	99.9(4)	126.9(5)	[17]
[Cu CN·(NEt$_3$)]	2.21(1)	101.6(4)	109.6(4)	[17]
[(Cu CN)$_3$·4(pip)]	2.183(9)	100.08(6)	116.06	[15]
[Cu$_2$(CN)$_2$·2(4-Acpy)]	2.09(2)–2.10 (2)	105.85(9)	106.39(9)	[13]
[Cu$_2$(CN)$_2$·2(3-Acpy)]	2.098(2)	99.66(9)	119.22(11)	[13]
[CuCN·0.5(tmpy)]	2.070(3)	86.70(12)	130.58(14)	[12]
[Cu$_2$(CN)(IN)(HIN)]$_n$	1.947(9)	155.0(3)	155.71(3)	[19]
[CuCN·EIN]	2.077	99.78(4)	121.56(11)	Current

Current means this study

Table 6 The wavenumbers (Cm-1) of different vibrational modes of **1**

Compound	$v_{(CH)}$ (arom.)	$v_{(CH)}$ (aliph.)	$v_{(C \equiv N)}$	$v_{(C=O)}$	$v_{(C=N)}$ and $\gamma_{(C=C)}$ (arom.)	δ_{CH} of L	γ_{CH} of L	v_{Cu-C}
[CuCN·EIN]	3035	2989 m, 2916 m	2121 s	1727 s	1608 s–1559 m 1467 s	1410 s	770 s 790 s	431w

W weak, *m* medium, *s* strong

3.2 Infrared Spectrum of 1

The IR spectrum of **1** exhibits bands characteristic of the (CuCN)$_n$ fragment and the EIN ligand (Table 6). The IR spectrum of 1 displays the bands of the EIN ligand at 3035 cm^{-1} ($v_{CH(arom)}$), 2989, 2916 cm^{-1} ($v_{CH(aliph.)}$), 1410 cm^{-1} (δ_{CH}) and 790 and 770 cm^{-1}(γ_{CH}). These bands are shifted to lower wave numbers from the vibrational frequencies of the free ligand due to the formation of hydrogen bonds between the hydrogen atoms of the ligands and the donor sites of the (CuCN)$_n$ fragment [26]. In contrast, the band in **1** at 1608 cm^{-1} corresponds to $v_{C=N}$ while those at 1559, 1467 and 1410 cm^{-1} are attributed to $v_{C=C}$ of the EIN ligands. These bands exhibit small shifts to lower wave numbers (6, 4 and 5 cm^{-1}, respectively) from those of the EIN ligand, hence supporting coordination of EIN to Cu(I).

Also, the IR spectrum of **1** shows a strong band at 1727 cm^{-1} due to $v_{C=O}$, which shifts to lower wave number relative to the carbonyl group of the free ligand (1738 cm^{-1}) due to the formation of hydrogen bonds.

It is noteworthy that the $v_{C \equiv N}$ band of **1** (2121 cm^{-1}) is different from that in K$_3$[Cu(CN)$_4$] (2081 cm^{-1}), which supports the presence of one type of cyanide group. In addition, the v_{Cu-C} band at 431 cm^{-1} confirms the presence of the (CuCN)$_n$ fragment.

3.3 Thermogravimetric Analysis

The thermogram of **1** shows three degradation steps. The first and the second steps are at 100–200 °C and at 450–540 °C, respectively, and correspond to the release of the EIN ligand (M.W = 63%). The first step involves removal of the carboethoxy group (COOC$_2$H$_5$); $\Delta m\%$ obser. (calc.) 30.5 (30.3). The second step is due to the release of the pyridyl moiety of the EIN ligand; $\Delta m\%$ obser. (calc.) 32.5 (32.4). At 850–900 °C the weight loss is due to the decomposition of the cyanide group; $\Delta m\%$ obser. (calc.) 10.5 (10.8). The molecular weight of the residue obtained after complete thermolysis of **1** under nitrogen atmosphere is coincident with metallic copper, $\Delta m\%$ obser. (calc.) 26.8 (26.4).
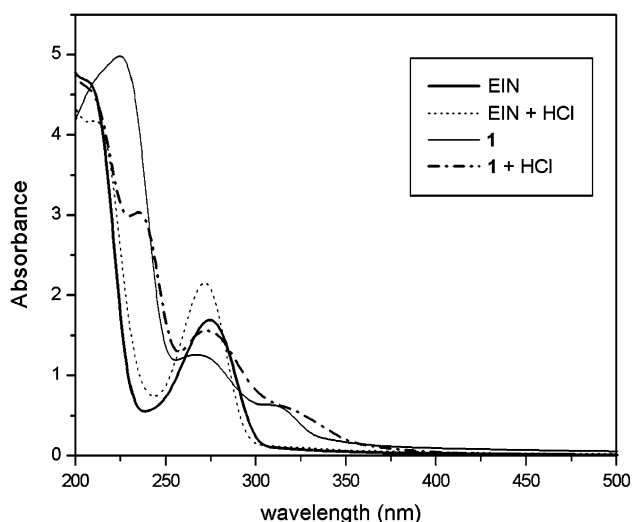
The thermogravimetric analysis of **1** indicates that the formula of **1** contains stable CuCN chains up to 850 °C while the EIN ligands evolve at relatively high temperatures indicating that the EIN molecules are strongly tied in the 3D-network via hydrogen bonds and strong coordination to the Cu(1) atoms as was previously supported by the crystal structure.

3.4 Electronic Absorption and Emission Spectra of 1

The electronic absorption spectra of EIN as a liquid in absence and presence of HCl reveal three and two bands, respectively, between 220 and 320 nm (Table 7). The high intensity band at 220 nm corresponds to $^1L_a \leftarrow {}^1A$ transition while that at 275 nm is due to $^1L_b \leftarrow {}^1A$ transition [27]. These bands resemble those of benzene, which exhibit a red shift upon substitution [27]. The long wavelength band at 320 nm may be assigned to a n-π* transition, which disappears in presence of HCl (Fig. 6).

Table 7 Absorption and emission bands of **EIN** and **1**

Compound	λabs (nm) in absence of HCl	λabs (nm) in presence of HCl	Assignment	λem (nm) in solid state
EIN	220	222	$^1L_a \leftarrow {}^1A$	–
	275	272	$^1L_b \leftarrow {}^1A$	–
	320	–	$n\text{-}\pi^*$	–
[CuCN, EIN],1	210	210	^1La	410
	225	235	CT	426
	272	275	^1L_b	462
	315	325	CT	487
				530

Fig. 6 Electronic absorption spectra of **EIN** and **1** in ethanol in absence and presence of HCl

The electronic absorption spectra of **1** in ethanol in presence and absence of HCl show four absorption bands between 210–325 nm (Table 7; Fig. 6). The ^1La band at 210 nm suffers a blue shift compared to EIN due to coordination to the copper site and the formation of different types of hydrogen bonds. However, the ^1L_b band appears near the same position at 275 nm. Two new bands appear in the spectra of **1** at 225–235 nm and at 315–325 nm due to MLCT and LMCT, respectively; and, the band due to n-π^* transition disappears due to coordination of EIN to the copper site.

Solid-state luminescent materials currently have potential applications in device displays, mainly as molecular sensing systems [28]. Thus, the luminescence of **1**, CuCN and EIN were studied in solid state and in solution. The emission spectrum of EIN has no bands in ethanolic solution on excitation at 280 nm. This finding is expected since pyridine and its derivatives are, generally, not
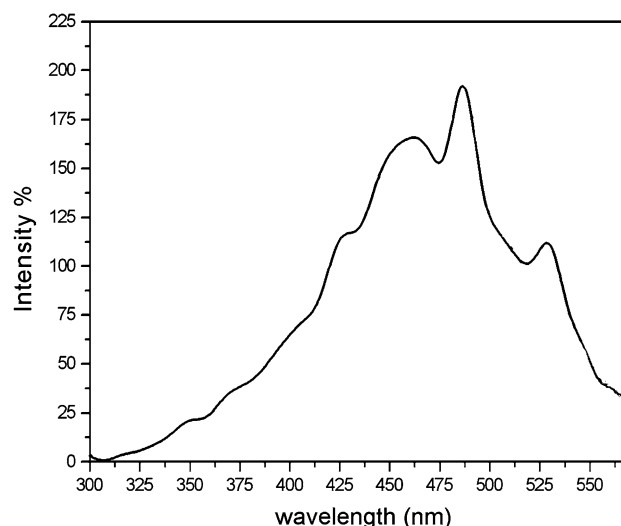
Fig. 7 Emission spectrum of **1** in solid state at excitation wavelength 280 nm

luminescent materials [29]. In contrast, the emission spectrum of **1** in the solid state reveals distinct high and low energ peaks in the visible region (390–530 nm) upon excitation at 280 nm (Fig. 7; Table 7). In this case, the luminescence may be discussed based on a number of possible photophysical transitions due to the CuCN chains, which are affected by coordination to EIN molecules. The emission spectrum of CuCN in solid-state shows broad bands at 400–545 nm on excitation at 280 nm.

Until recently, the luminescence of CuCN was unstudied. Based on TD-DFT calculations, the emission spectrum was assumed to arise from transitions between the lowest excited triplet state and the ground state singlet [30]. The S_o-T gap for the bent triplet chains is consistent with emission wavelength for bulk CuCN [29]. Since the emission spectrum of **1** resembles that of CuCN, it is apparent that the luminescence of **1** is caused by transitions within the CuCN chains, while the observed red shift and relatively high intensity relative to that of CuCN is due to coordination to EIN to form a 3D-network [31]. The luminescence excitation in **1** could be caused by different possible transitions including metal-to-ligand charge transfer (MLCT), metal cluster-centered (CC) transitions, single-metal-centered (MC) transitions and ligand-centered (LC) transitions. Since, cyanide and EIN have large band gaps, they are ruled out. The absence of close Cu···Cu contacts in **1**, where the nearest Cu···Cu distance is 3.913 Å, argues against CC transitions. Elimination of the LC and CC phenomena leaves the MC transition and MLCT as possible photophysical sources of luminescence behavior in **1**.

The emission spectrum of **1** is assumed to arise from transitions from the lowest excited-triplet state to the

ground state. Lifetime studies of soluble Cu(I)-cyano species have suggested that emission is usually a phosphorescence phenomenon [32–35]. The red shift and the relatively high intensity of the emission bands of **1** relative to CuCN may be due to three-coordinate copper centers and the bent structure of the CuCN chains, which allow for the distortion that is obtained in the bent triplet structures, which produce multiple triplet states [30].

4 Appendix A. Supplementary Data

CCDC 767192 contains the supplementary crystallographic data for **1**. These data can be obtained free of charge via http://www.ccdc.cam.ac.uk/conts/retrieving.html, or from the Cambridge Crystallographic Data Centre, 12 Union Road, Cambridge CB2 1EZ, UK; fax: (+44) 1223-336-033; or e-mail: deposit@ccdc.cam.ac.uk.

References

1. A.M. Peedikakkal, J.J. Vittal, Inorg. Chem. **49**, 10 (2010)
2. R.J. Kuppler, D.J. Timmons, Q.-R. Fang, J.-R. Li, T.A. Makal, M.D. Young, D. Yuan, D. Zhao, W. Zhuang, H.-C. Zhou, Coord. Chem. Rev. **253**, 3042 (2009)
3. B.H. Ye, M.L. Tang, X.M. Chen, Coord. Chem. Rev. **249**, 545 (2005)
4. Z. Su, K. Cai, J. Fan, S.S. Chen, M.S. Chen, W.Y. Sun, Cryst. Eng. Comm. **12**, 100 (2010)
5. L.F. Ma, L.Y. Wang, M. Du, S.R. Batton, Inorg. Chem. **49**, 365 (2010)
6. J. Lee, O. K. Farha, J. Roberts, K. A. Scheidt, S. T. Nguyen, J. T. Hupp, Chem. Soc. Rev. **38**, 1450 (2009)
7. M.D. Allendorf, C.A. Bauer, R.K. Bhakta, R.J.T. Houk, Chem. Soc. Rev. **38**, 1330 (2009)
8. M. Sabo, A. Henschel, H. Froede, E. Klemm, S. Kaskel, J. Mater. Chem. **17**, 3827 (2007)
9. Y.K. Hwang, D.-Y. Hong, J.-S. Chang, S.H. Jhung, Y.-K. Seo, J. Kim, A. Vimont, M. Daturi, C. Serre, G. Férey, Angew. Chem. Int. Ed. **47**, 4144 (2008)
10. S. Ma, H.-C. Zhou, Chem. Commun. **46**, 44 (2010)
11. Q.-G. Zhai, S.-N. Li, X. Gao, W.-J. Ji, Y.-C. Jiang, M.-C. Hu, Inorg. Chem. Commun. **13**, 211 (2010)
12. S.E.H. Etaiw, S.A. Amer, M.M. El-bendary, J. Mater. Sci. **45**, 1307 (2010)
13. S.E.H. Etaiw, S.A. Amer, M.M. El-bendary, Polyhedron **28**, 2385 (2009)
14. U.S. Schubert, C. Eschbaumer, Angew. Chem. Int. Ed. **4**, 2829 (2004)
15. G.A. Bowmaker, C. Pettinari, B.W. Skelton, N. Somers, N.A. Vigar, A.H. White, Z. Anorg. Allg. Chem. **633**, 415 (2007)
16. G.A. Bowmaker, K.C. Lim, B.W. Skelton, A.H. White. Z. Naturforsch **59b**, 1264 (2004)
17. J.C. Dyason, P.C. Healy, L.M. Engelhardt, C. Pakawatchai, V. A Patrick, A.H. White. J. Chem Soc. Dalton Trans., 839 (1985)
18. R. Sekiya, S. Nishikiori, K. Ogura, Inorg. Chem. **45**, 9233 (2006)
19. P. Amo-Ochoa, P. J. S. Miguel, O. Castilloc, F. Zamora, Cryst. Eng. Comm **9**, 987 (2007), and references therein
20. M.H. Yang, Acta Cryst. C **65**, m59 (2009)
21. P.Y. Cheng, C.Y. Chen, H.M. Lee, Inorg. Chim. Acta **362**, 1840 (2009)
22. A.M. Beatty, CrystEngComm **51**, 1 (2001)
23. H.H.-Heidl, S.E. H. Etaiw, M. Sh. Ibrahim, A.S. B. El-din, R.D. Fischer, J. Organomet. Chem. **684**, 329 (2003), and references therein
24. J.W. Eastes, W.M. Burgess. J. Am. Chem. Soc. **64**, 1187 (1942)
25. D.T.Cromer, A.C. Larson, Acta Cryst. Sec. B **28**, 105 (1972)
26. A. Spalleti, G. Cruciani, U. Mazzucato, J. Mol. Struct. **612**, 339 (2002)
27. H. H. Jaffé, M. Orchin, Theory and Applications of Ultraviolet Spectroscopy, Fifth Printing (John Wily and Sons, Inc., 1970)
28. R. C. Ropp, *Luminescence and the Solid State*, 2nd edn (Elsevier, Amsterdam, 2004)
29. B. Valeur, *Molecular Fluorescence Principles and Applications*, (WILEY-VCH Verlag GmbH, 69469 Weinheim (Federal Republic of Germany, 2002), p. 59
30. C.A. Bayse, T.P. Brewster, R.D. Pike, Inorg. Chem. **48**, 174 (2009)
31. M.J. Lim, C.A. Murray, T.A. Tronic, K.E. deKrafft, A.N. Ley, J.C. deButts, R.D. Pike, H. Lu, H.H. Patterson, Inorg. Chem. **47**, 6931 (2008)
32. A. Horváth, K.L. Stevenson, Inorg. Chem. **32**, 2225 (1993)
33. A. Horváth, C.E. Wood, K.L. Stevenson, Inorg. Chem. **33**, 5351 (1994)
34. K.L. Stevenson, J.H. Jarboe, S.A. Langmeyer, T.W. Acra, Inorg. Chem. **42**, 3559 (2003)
35. A. Horváth, Z. Zsilák, S. Papp, J. Photochem. Photobiol. A **50**, 129 (1989)